Journal of Achievements in Materials and Manufacturing Engineering
VOLUME 37
ISSUE 2
December
2009

The influence of sintering time on the properties of PM duplex stainless steel

Z. Brytan [a,*], L.A. Dobrzański [a], M. Actis Grande [b], M. Rosso [b]
[a] Division of Materials Processing Technology, Management and Computer Techniques in Materials Science, Institute of Engineering Materials and Biomaterials, Silesian University of Technology,ul. Konarskiego 18a, 44-100 Gliwice, Poland
[b] Department of Materials Science and Chemical Engineering, Politecnico di Torino Alessandria Campus, Viale T. Michel 5, 15100, Italy
* Corresponding author: E-mail address: zbigniew.brytan@polsl.pl

Received 21.09.2009; published in revised form 01.12.2009

Properties

ABSTRACT

Purpose: The purpose of this paper is to analyse the effect of sintering time on the pore morphology, microstructural changes, tensile properties and corrosion resistance of vacuum sintered duplex stainless steel.
Design/methodology/approach: In presented study PM duplex stainless steels were obtained through mixing base ferritic stainless steel powder with controlled addition of elemental alloying powders and then sintered in a vacuum furnace with argon backfilling at 1250°C for different time periods. Produced materials were studied by LOM/SEM metallography and the pore morphology was characterized. The mechanical properties were studied in tensile, hardness and Charpy impact tests. The corrosion resistance was evaluated by means of salt spray test and immersion in sulfuric acid.
Findings: Prolongation of sintering time influenced on increase of density thus on the mechanical properties and microstructure balance.
Practical implications: Mechanical properties of obtained PM duplex stainless steels are very promising, especially with the aim of extending their field of possible applications.
Originality/value: The possibility of obtaining balanced austenitic-ferritic microstructure of stainless steel using elemental powders added to a stainless steel base powder. The vacuum sintering of such powder mixture results in good microstructural homogeneity.
Keywords: Powder metallurgy; Sintering; Duplex stainless steel

Reference to this paper should be given in the following way:
Z. Brytan, L.A. Dobrzański, M. Actis Grande, M. Rosso, The influence of sintering time on the properties of PM duplex stainless steel, Journal of Achievements in Materials and Manufacturing Engineering 37/2 (2009) 387-396.

1. Introduction

PM stainless steels permanently represent a very interesting field for research, especially the multiphase stainless steels like duplex ones which show attractive combination of mechanical strength and corrosion resistance related to their austenite-ferrite microstructure. Manufacturing of duplex stainless steels by PM presents some advantages regarding to low production costs and possibility of integration, in one sintering cycle the sintering and heat treatment steeps, like when sinter-hardening process is applied, as in presented paper [1-3].

Duplex stainless steels made by addition of alloying elements to single-phase stainless steel powder and sintering in vacuum have proved adequate duplex microstructure with good mechanical and corrosion properties [4-6]. The mechanical and corrosion properties of PM stainless steel compared to wrought alloys are lower due to presence of porosity. The proper evaluation and control of this feature can be determinative for final properties of the sintered material [7-9].

The evaluation of pore morphology can be done by means of image analysis on unetched metallographic sections. Such approach was applied in [10] for investigation on influence of the sintering temperature on the pore characteristic and more recently in [11]. Both studies for the pore morphology description used with success the equivalent ellipse concept developed and described in [12]. In the present study similar approach to use pore shape factors for porosity characterization was applied. Moreover, the influence of sintering time on the mechanical and corrosion performance of PM duplex stainless steel was studied.

2. Experimental procedure

In order to produce sintered duplex stainless steel the ferritic stainless steel powder 430LHC (16.86%Cr, 1.15%Si, 0.18%Mn, 0.02%C) manufactured by Hoganas Corporation was used as starting base powder and then it was mixed with addition of alloying elements powders such as ferrochromium powder Fe-Cr, Ni and Mo in the right quantity to obtain the chemical composition similar to duplex stainless steel.

The chemical composition of prepared powder mixture (table 1) was calculated using Schaeffler's diagram, where the chromium and nickel equivalents were count, thus Cr_{eq}=%Cr+%Mo+1.5%Si and Ni_{eq}=%Ni+0.5%Mn+30%C. A chemical composition of produced mixture was placed in austenitic-ferritic area of the Schaeffler's diagram. Naturally isothermal projected phase diagram of ternary Fe-Cr-Ni system was taken into consideration and the proper range of coexistence of both phases was controlled theoretically.

During the composition preparation lubricant Acrawax was used in a quantity of 0.65 wt. %. Premix was mixed in Turbula mixer for 20 min and then compacted at 700MPa in the form of dog bone samples for tensile test and bars samples according to Charpy impact test. Prior to the sintering step a dewaxing process was performed at 550°C for 60 minutes in a nitrogen atmosphere. Samples were then sintered in a vacuum furnace with argon backfilling at 1250°C for different periods varying from 1 to 4 hours. After sintering rapid cooling was applied using nitrogen under pressure of 6bar (0.6MPa) with cooling velocity of about 6ºC/s calculated in range 1250-400°C.

Microstructure observations were carried out on the light optical microscope (LEICA ME F4M) and the scanning electron microscope (SEM) LEO 1450 VP with the EDS probe. The porosity of materials has been investigated on a non-etched metallographic section using Leica Qwin image analysis system. Characterization was carried out at magnification of 200x on 10 different image fields, thus at least 5000 pores were processed. The stereological parameters like f_s and f_c were measured individually for each pore to describe its dimensional and morphological characteristic. Moreover pores diameters D_e were measured. The pore shape factor f_s describe pore elongation in the plain of analysis and was calculated according to formula (1), where d_{min} and d_{max} are minimum and maximum Feret diameter of a pore. The pore shape factor f_c represent the pore profile irregularity and was calculated according the formula (2), where A and P are respectively the area and the perimeter of metallographic cross-section of pore.

$$f_s = d_{min} / d_{max}, \quad (1)$$

$$f_c = 4\pi A / P^2, \quad (2)$$

The shape factor of 1 represents a circular pore in the plane of analysis and as the number decreases from 1, the degree of irregularity increases. The calculations included only pores of area > 9 μm and < 50 μm.

Table 1.
The average chemical composition of studied powder mixture

Elements concentration, wt. %						Cr_{eq}	Ni_{eq}	Cr_{eq}/Ni_{eq}
Cr	Ni	Mo	Si	Mn	C			
22.48	6.00	3.00	0.95	0.14	0.02	28.34	6.54	4.33

The evaluation of phase composition was made using X-ray diffractometer with the filtered copper lamp rays of CuKα and an acceleration voltage of 40kV and heater current of 40mA. The measurements were made in diffraction angle 2θ from 40 to 100°. The phase quantity was estimated using Averbach and Cohen method of direct comparison assuming that $V_\gamma + V_\alpha = 1$ [13].

Density was evaluated using the water displacement method. Mechanical properties were evaluated basing on the tensile test performed according to EN 10002-1 standard on samples prepared according to ISO 3928. The Charpy impact test was made on un-notched samples according to EN 10045. The hardness was measured in HRA scale. Fracture analysis was carried out on the tensile tested samples after fracture. Corrosion properties were studied through salt spray test according to BSI 7479:1991 in 5%NaCl solution and immersion test in 5M H_2SO_4 solution.

3. Results and discussion

3.1. Porosity

The Figures 1 and 2 shows non-etched images of samples sintered for 1 and 4 hours of studied composition. The density was increased from 7.14 g/cm^3 for 1h of sintering time to 7.24 for 2h and successively to 7.30 and 7.40 for 3h and 4h respectively.

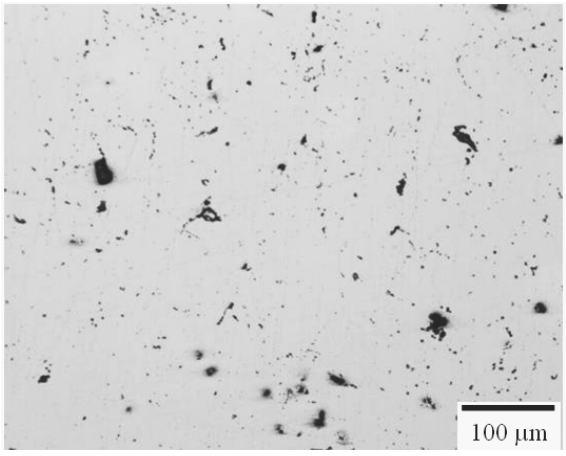

Fig. 1. Typical porosity after sintering for 1h, ρ=7.14g/cm^3

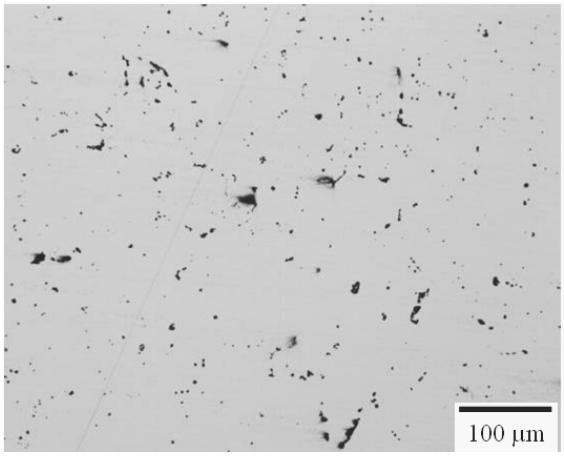

Fig. 2. Typical porosity after sintering for 4h, ρ=7.4g/cm^3

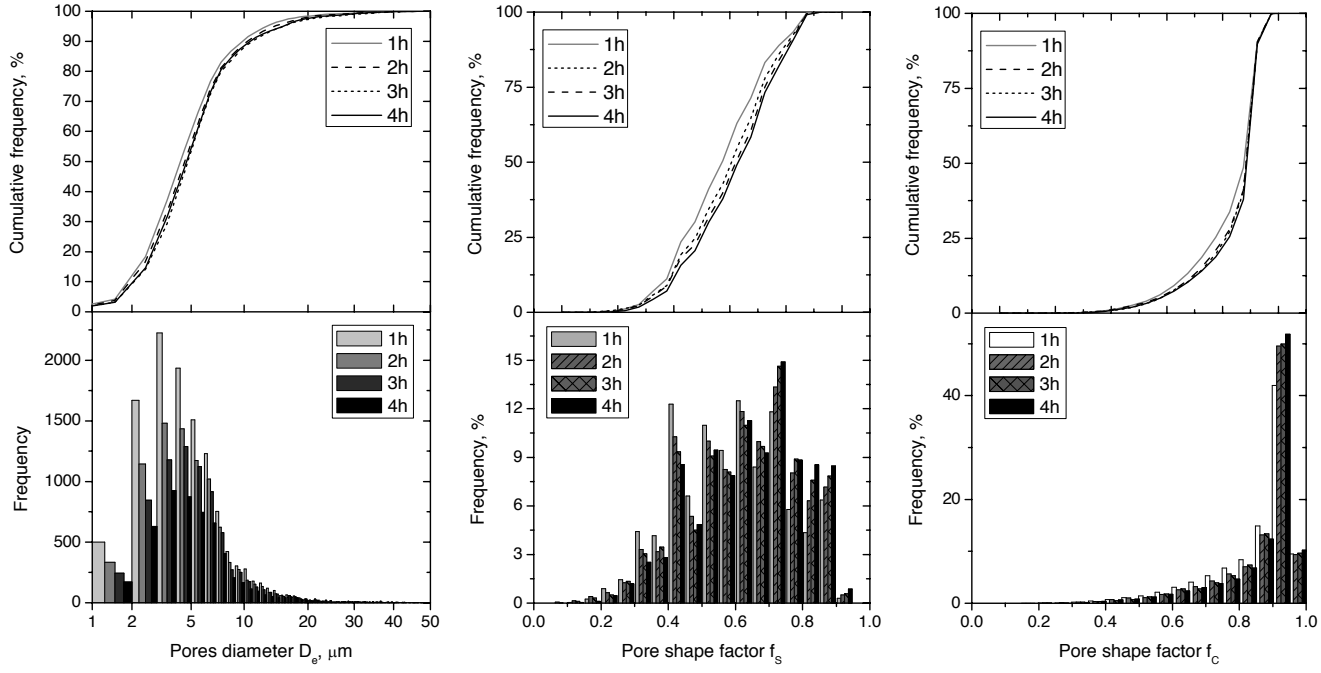

Fig. 3. Cumulative frequency function and frequency distribution of pores diameter D_e and pore shape factors f_s, f_c in microstructure of studied composition sintered in the range of 1 to 4 hours

Figure 3 shows the distribution of pore diameters and pore shape factors for studied composition sintered in the range of 1 to 4 hours. The diameters of analysed pores where mainly included in the range of 2-40µm and about 90% of them were smaller than 10µm. Prolonged sintering time reduced uniformly portion of each size pores. The effect of sintering cycle on pore morphology is more evident in the pore shape factor f_s than f_c, that both are shifted towards higher values that confirm lower pore elongation and their higher regularity with prolonged sintering time. The mean value of f_s after 1h sintering was 0.591 and increased to 0.640 after 4 hours of sintering while the f_c varied from 0.847 to 0.868. Variations of pore shape factors during sintering are more evident when shorter sintering time is analysed i.e comparing pore morphology after sintering in the range of 0.5-2h, previously described in [6].

The distribution of f_s and f_c values as a function of pores diameters are shown in Figures 4 and 5 for studied composition sintered for 1 and 4 hours, respectively. The analysis of the pore distribution shows that no considerable differences of pores shape factors related to pore diameter take place when sintering with various conditions. The pore shape factors remain not influenced by the pore diameter; in both cases the majority of values are

located up to 20μm of pore diameter. The prolonged sintering time decrease the number of pores with low f_c and overall number of pore population that after 4h of sintering shows predominantly high values of f_c.

Figure 6 shows the distribution of pore shape factor f_s versus f_c and D_e. According to equivalent ellipse concept described in [12] the solid line on the figure represents equivalent ellipse i.e. for every f_s the upper limit of corresponding f_c. Analysing this morphology map, it can be seen that distribution of registered values is located near the theoretical ellipse. Registered pore diameters show uniform distribution along all measured experimental points when sintered for 1h, while for 4h the porosity of higher dimension is preferentially located at the vicinity of theoretical ellipse - at f_c maximum for given f_s.

The previously described effects of pore geometry, together with increasing mean pore area from 40.47μm^2 for 1h to 56.51μm^2 after 4h sintering confirm the trend to improve pore morphology. The influence of sintering time on the pore morphology is more evident when comparing pore geometry for 1h and 2h rather than for longer sintering cycles (Fig. 7). Moreover, the increase of sintering time has a higher influence on the pore profile irregularity (expressed by f_s) than on the macroscopic shape given by shape factor f_c.

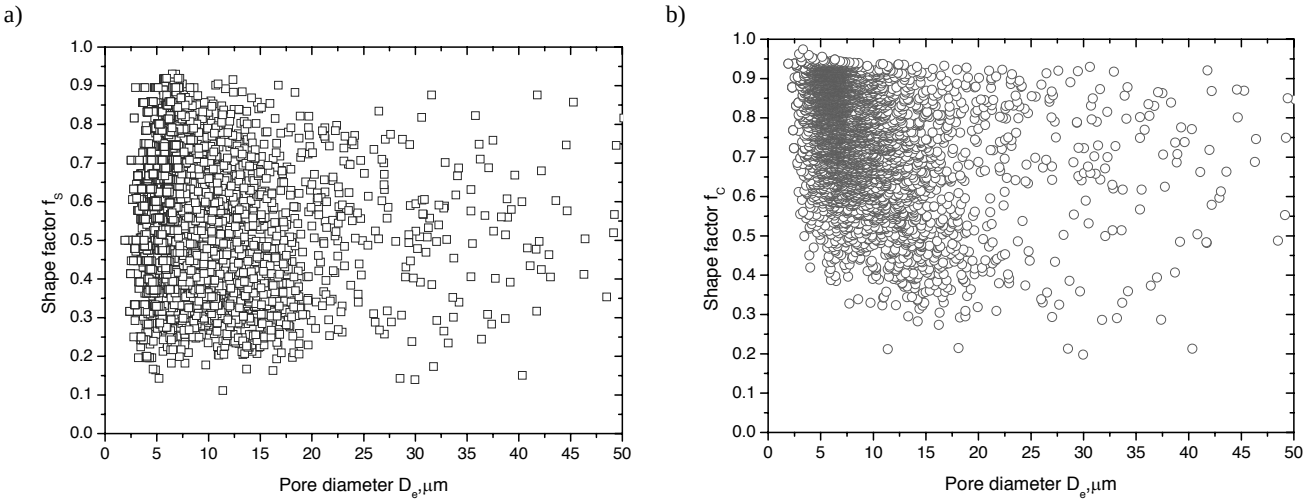

Fig. 4. The distribution of pore shape factor a) f_s and b) f_c versus pore diameter D_e for studied composition sintered for 1 hour

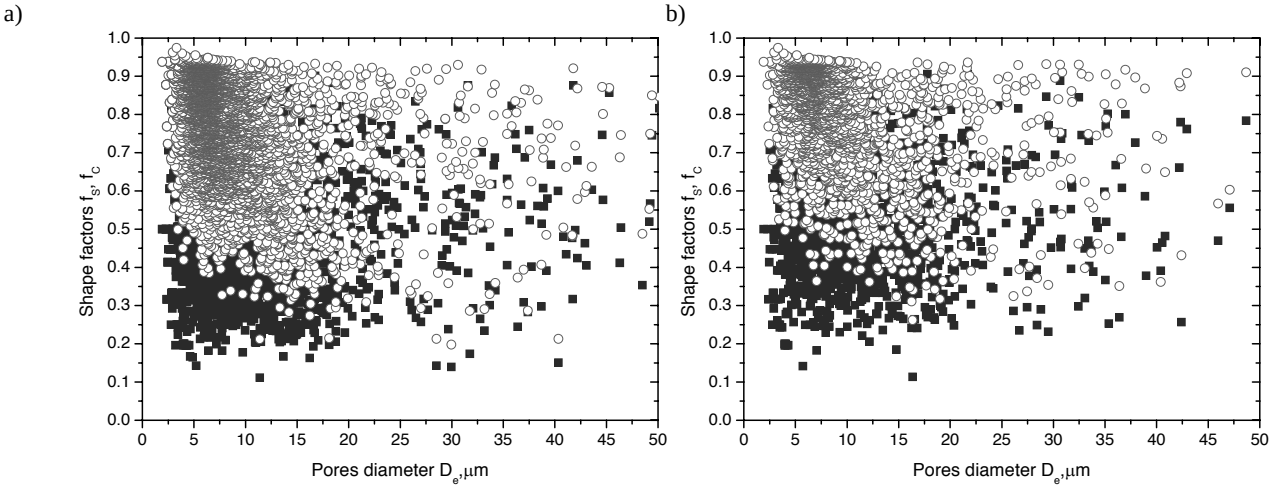

Fig. 5. The distribution of pore shape factors f_s, f_c versus pore diameter D_e for studied composition sintered for a) 1h and b) 4 hours

a) b)

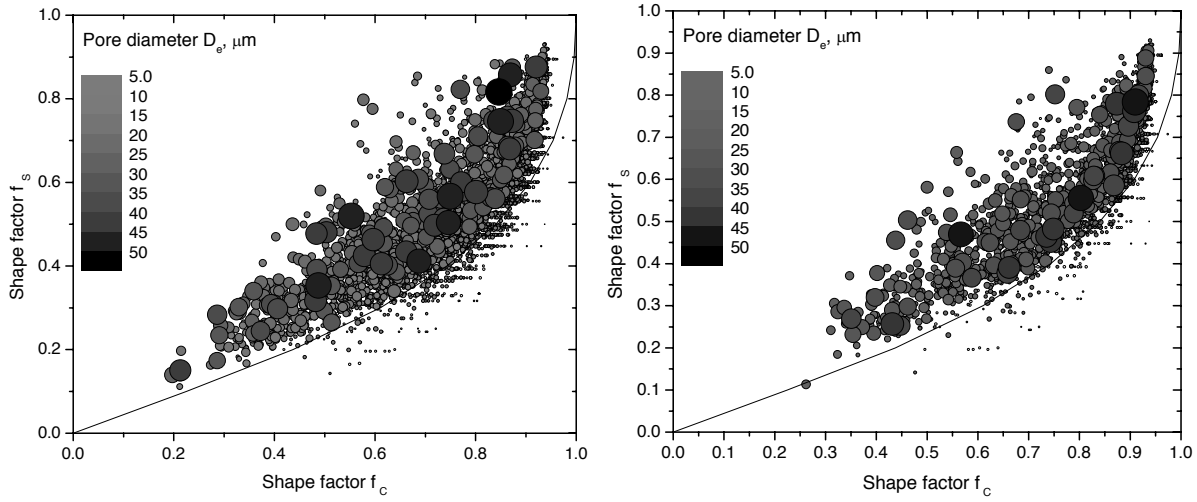

Fig. 6. The distribution of pore shape factor f_s versus pore shape factor f_c and D_e for studied composition sintered for a) 1h and b) 4 hours

Figure 6 shows the distribution of pore shape factor f_s versus f_c and D_e. According to equivalent ellipse concept described in [12] the solid line on the figure represents equivalent ellipse i.e. for every f_s the upper limit of corresponding f_c. Analysing this morphology map, it can be seen that distribution of registered values is located near the theoretical ellipse. Registered pore diameters show uniform distribution along all measured experimental points when sintered for 1h, while for 4h the porosity of higher dimension is preferentially located at the vicinity of theoretical ellipse - at f_c maximum for given f_s.

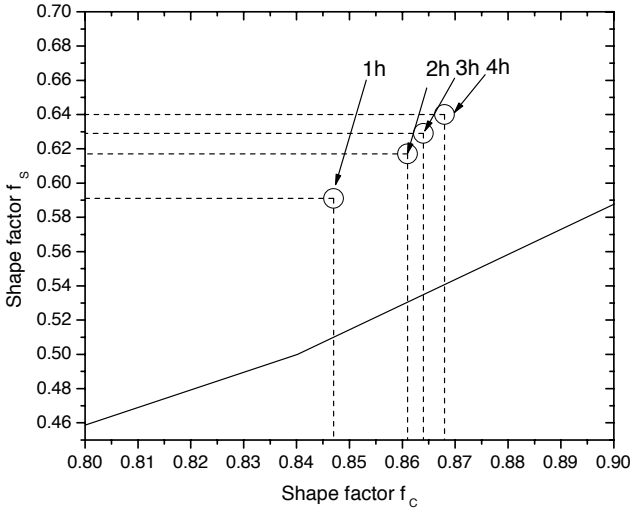

Fig. 7. The medium value of pore shape factor f_s versus pore shape factor f_c depend on sintering time.

The previously described effects of pore geometry, together with increasing mean pore area from 40.47µm^2 for 1h to 56.51µm^2 after 4h sintering confirm the trend to improve pore morphology. The influence of sintering time on the pore morphology is more evident when comparing pore geometry for 1h and 2h rather than for longer sintering cycles (Fig. 7). Moreover, the increase of sintering time has a higher influence on the pore profile irregularity (expressed by f_s) than on the macroscopic shape given by shape factor f_c.

3.2. Microstructure development

The study of microstructures of sintered duplex stainless steel revealed the biphasic austenitic-ferritic microstructure with heterogeneously distributed phases, both ferrite - bright and austenite - dark.

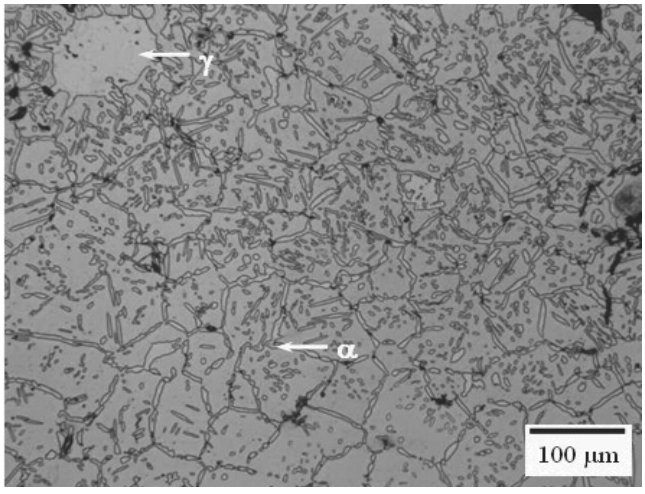

Fig. 8. The microstructure of duplex stainless steel sintered for 1 hour (LOM)

Duplex stainless steel sintered for 1h consists of ferritic matrix where the growth of austenitic phase proceeds through grain boundaries.The zones of massive austenite were also present. The austenite in all analysed materials is located along prior ferritic grain boundaries on the primary powder particles contact surfaces and occur as intra-granular austenite side plates.Prolonged sintering time results in liquidation of massive austenitic zones and progressive development of cellular austenite grains, as shown in Figures 8-9. The small acicular grains of austenite start to grow inside mutual connected primary austenitic zones (Fig. 10). The Figure 11 presents austenitic sub-grains of a mean dimension of 7μm growing inside primary ferritic region in the stainless steel microstructure sintered for 4h.

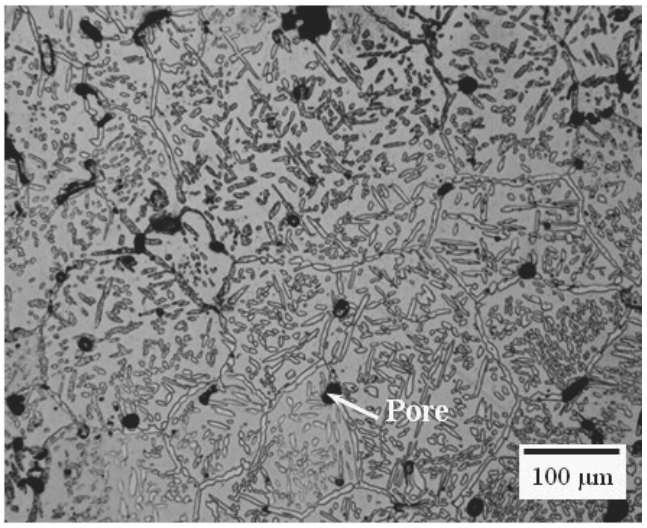

Fig. 9. The microstructure of duplex stainless steel sintered for 4 hours (LOM)

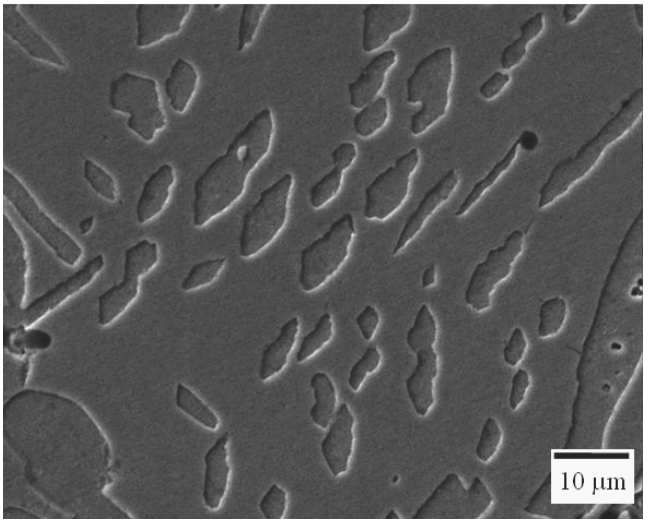

Fig. 10. SEM micrograph of austenitic sub-grains in microstructure of sintered stainless steel for 2h

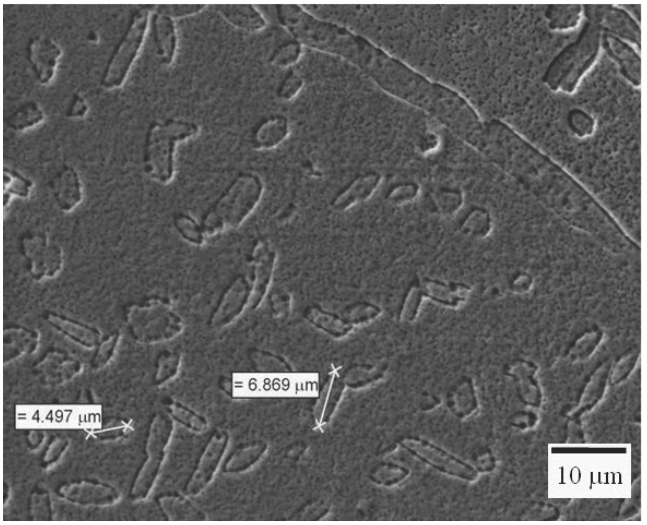

Fig. 11. SEM micrograph of austenitic sub-grains in microstructure of sintered stainless steel for 4h

The diffraction analysis of sintered stainless steel confirmed the presence of austenitic and ferritic phases (Fig. 12). The diffraction peaks origin of austenite Fe γ (111), (200), (220), (222), (311) and ferrite Fe α (110), (200), (211), (220) were clearly identified from x-ray patterns for all sintered conditions. Prolongation of sintering time result in increase of Feα peak intensity, thus the quantity of ferrite was increased from 31% to 49% in the range of sintering time from 1 to 4 h. It can be noted that sintering for 1 and 2h has lower influence of the phase balance than sintering for 3h. Further prolongation of sintering time to 4h doesn't influence on the ferrite content considerably; the increase is only about 2%. Sintering for 3 hours seems to be optimal at least for the formation of a balanced microstructure.

The EDS microanalyses were carried out in austenitic and ferritic regions of sintered duplex stainless steel microstructure (Table. 2). The concentration of Ni is higher in austenitic regions than in ferritic, which are enriched in ferrite former elements like Cr and Mo. Element partitioning between both phases is consistent with the stabilizing effect of each element on the respective phase. Detailed EDS studies of both phases revealed that increase of sintering time have not influenced significantly on the partition coefficients for a given element. Table 3 presents the partition coefficients (k = ferrite / austenite) as the product of average concentration of given element in the α an γ phases individually. During sintering between 1 to 4 hours the partition coefficient of Cr (k_{Cr}) is close to 1.2 and of molybdenum (k_{Mo}) about 1.5 while the nickel partition coefficient (k_{Ni}) about 0.6. As the sintering time grows, the partition coefficients of ferrite former elements (Cr, Mo) tend to increase, which is more evident in the case of (k_{Mo}), increasing from 1.43 to 1.58. The opposite effect is evident for nickel partition coefficient (k_{Ni}), as shown on Fig. 13.

The development of austenitic-ferritic microstructure in analysed conditions is mainly driven by diffusional processes during sintering, so with prolonged sintering time both austenite and ferrite former elements segregates in respective phases and their concentration become higher.

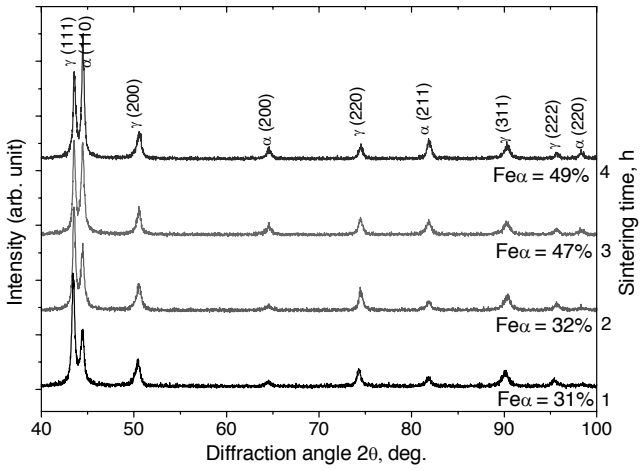

Fig. 12. The x-ray diffraction patterns of duplex stainless steel sintered for different time periods and corresponding quantity of ferritic phase

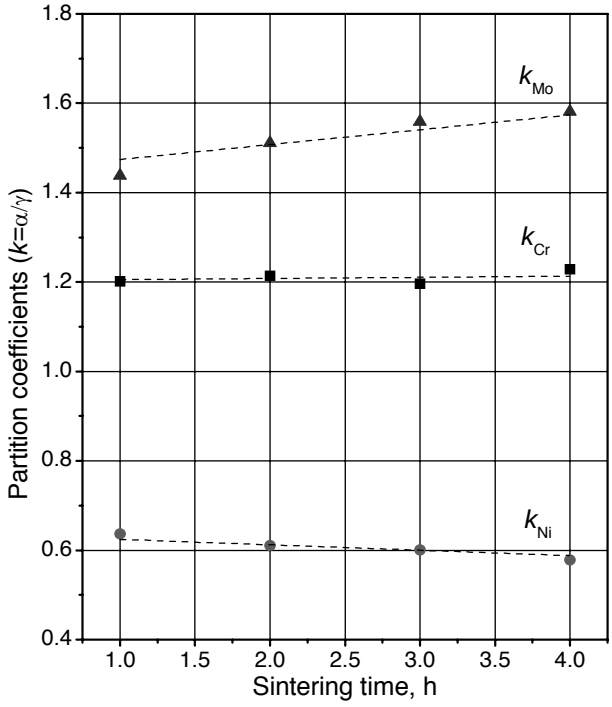

Fig. 13. The partition coefficients (k) of major alloying elements in duplex stainless steel sintered for different sintering times

3.3. Mechanical properties

The mechanical properties of sintered duplex stainless steels increase with prolonged sintering time and achieve very satisfactory characteristics in term of tensile and yield strength as well as elongation values (Fig. 14).

Table 2.
Average chemical composition of α and γ phases (wt. %)

Element	Phase	Sintering time, h				Stand. dev.
		1	2	3	4	
Si	α	1.32	1.31	1.38	1.40	±0.11
	γ	1.21	1.33	1.30	1.36	±0.11
Cr	α	28.69	28.26	29.22	29.70	±0.26
	γ	23.89	23.28	24.41	24.17	±0.25
Mn	α	0.42	0.44	0.43	0.42	±0.16
	γ	0.47	0.49	0.50	0.54	±0.16
Fe	α	61.25	61.19	59.91	59.39	±0.36
	γ	66.19	66.21	64.80	64.91	±0.37
Ni	α	2.81	2.93	3.12	3.22	±0.17
	γ	4.41	4.81	5.20	5.57	±0.20
Mo	α	5.53	5.87	5.89	5.90	±0.32
	γ	3.85	3.89	3.78	3.73	±0.32

Table 3.
Partition coefficients (k) of duplex stainless steel sintered for different sintering times

Partition coefficients	Sintering time, h			
	1	2	3	4
k_{Cr}	1.20	1.21	1.20	1.23
k_{Ni}	0.64	0.61	0.60	0.58
k_{Mo}	1.44	1.51	1.56	1.58

The composition sintered in this study after 1h obtains tensile strength of about 700MPa, yield strength of 680MPa at 14% of elongation. Tensile properties progressively increase with sintering time and for tensile and strength an increase of 7-8% was obtained after sintering for 4h if compared to 1h. Elongation improved of about the level of 23%. It must be remembered that the increase of mechanical properties does not only depend on density – strictly related to sintering time - but also on microstructure phase composition of analyzed sintered stainless steels. In addition to the density, the correct balance between austenitic and ferritic phase plays a decisive role when high mechanical properties are needed. At duplex stainless steel microstructure the strength is enhanced by increasing the volume fraction of ferrite which is stronger than austenite. Improvement of mechanical properties of sintered duplex stainless steels with higher ferrite content may be explained by the solid solution hardening of Ni and Mo in the ferrite phase. The internal strain hardening between ferrite and austenite, due to different coefficients of thermal expansion and refinement of the grain size cause the increase of tensile properties.

The influence of sintering time on impact strength and hardness is presented in Figure 15. The hardness values were slightly increased from 51 to 54 when sintered for 1 to 4h, while the impact strength raised more than 200% from 95J at 1h sintering to 150J and 227J for 2h and 4h of sintering, respectively. Obtained results are also in consistence with phase quantity of ferrite and austenite in the microstructure. The toughness of sintered duplex steel strongly depends on many structural factors like density, porosity distribution and shape of pores, basically because the pores act as places of stress concentration and crack initiation sites. Figure 16 shows curves of load against time

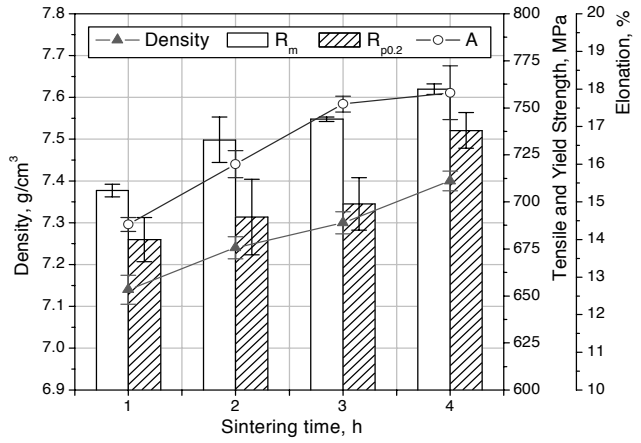

Fig. 14. The influence of sintering time on tensile properties of studied sintered duplex stainless steel

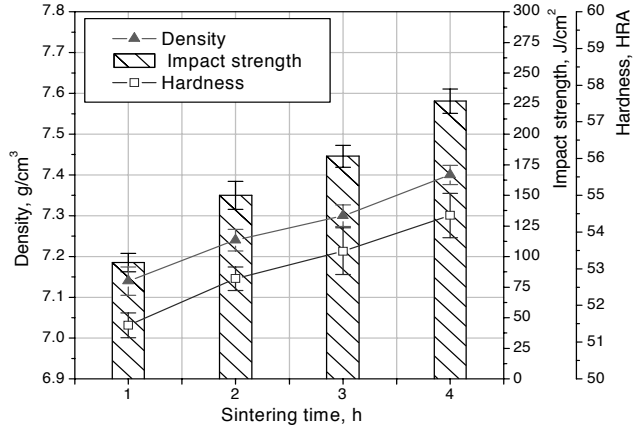

Fig. 15. The influence of sintering time on impact strength and hardness of studied sintered duplex stainless steel

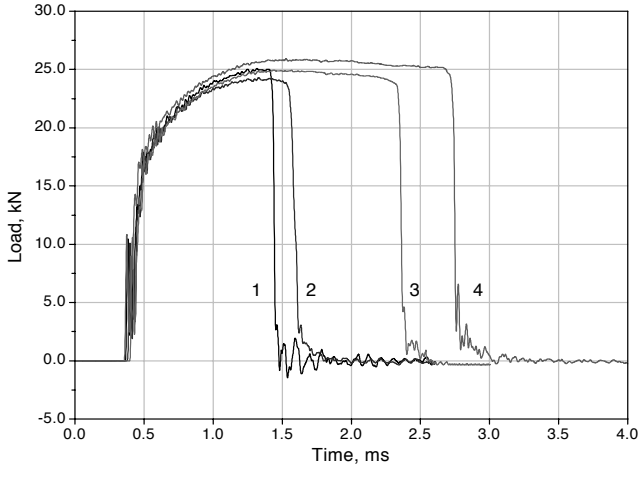

Fig. 16. The dynamic load time curves of samples sintered for different time periods (1, 2, 3 and 4 is sintering time in hours)

recorded by instrumented impact test. Longer sintering cycles result in slight increase of the maximum load, which is about 25kN for all tested conditions. The characteristic of dynamic load time curve for the samples sintered at 1 and 2 hours are similar and also samples sintered for 3h shows similar curve shape than those sintered for 4h. Elongation of sintering time in studied conditions causes an increase of connections between powder particles and improve pore morphology that have the greatest impact on the toughness.

The fractography analysis shows a mixed type of ductile and brittle fracture (Fig. 17). With prolonged sintering time the portion of plastic zones increase and dimples type rupture occurs. Fracture surface after 1h sintering is composed of small oval dimples located along plastic deformation zones (Fig. 17a), while for samples sintered for 4h the fracture surface is composed of large and elongated dimples oriented as the same direction as the loading (Fig. 17b).

a)

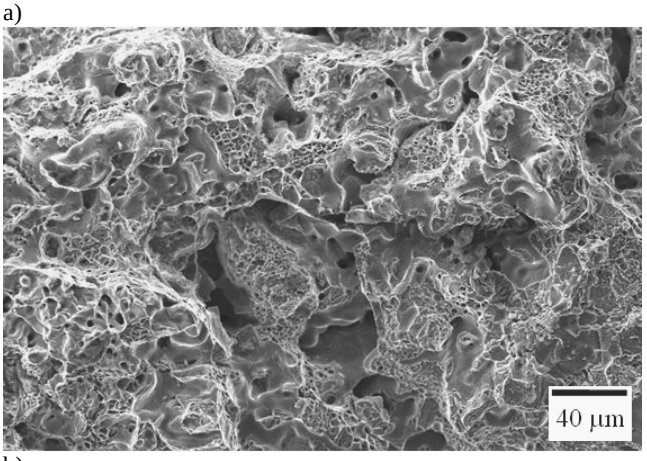

b)

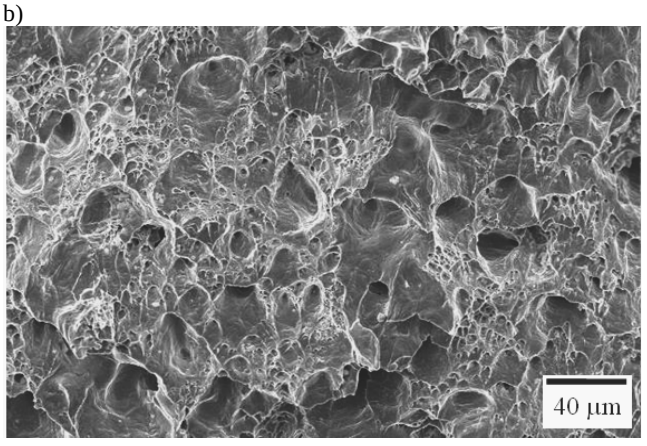

Fig. 17. SEM micrographs showing the fracture surface of a sample a) sintered for 1h and b) for 4h

3.4. Corrosion properties

The influence of sintering conditions on corrosion properties was characterized using salt spray test chamber, where Charpy

impact test samples were tested for 600h. The corrosion resistance was evaluated basing on portion of surface area attacked by corrosion or covered by corrosion products. Samples sintered for longer time periods exhibit lower corroded surface area in salt spray test (Fig. 18), where the porosity plays dominant role in corrosion initiation. As corrosion attack starts inside open pores and propagate through interconnected porosity inside the sample, the formation of corrosion products starts to be visible on surface, in form of brown tracks (Fig. 19). The samples surface was free of visible signs of new pits formation and the pitting corrosion was preceded only in already present surface porosity. The overall corrosion resistance of sintered duplex stainless steels in salt spray test depends on porosity; therefore after 600h of test samples sintered for 4h shows the lowest corrosion level <6% of corrodes surface, while other even 10 times more.

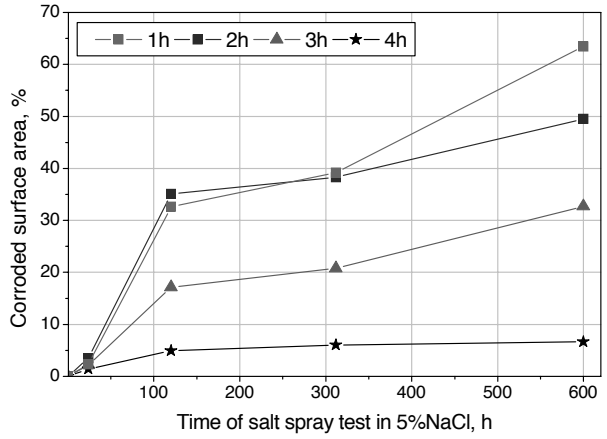

Fig. 18. Salt spray test results for samples sintered for different time periods

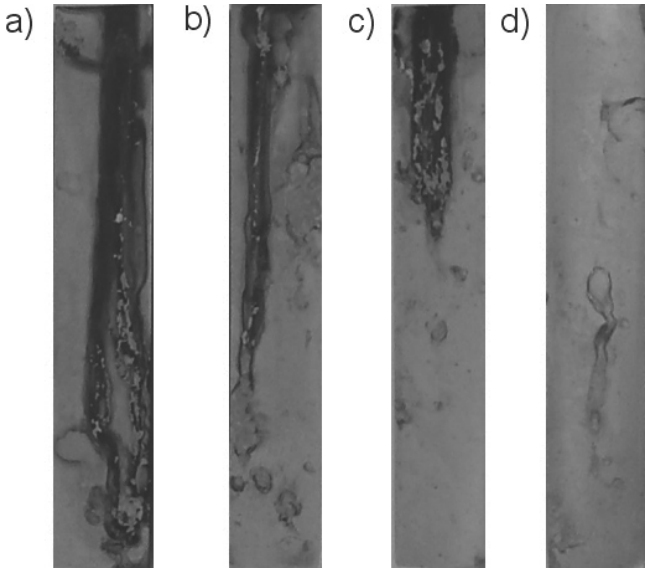

Fig. 19. Samples surface after 600h of salt spray test, a) sintered for 1h, b) 2h, c) 3h and d) for 4h

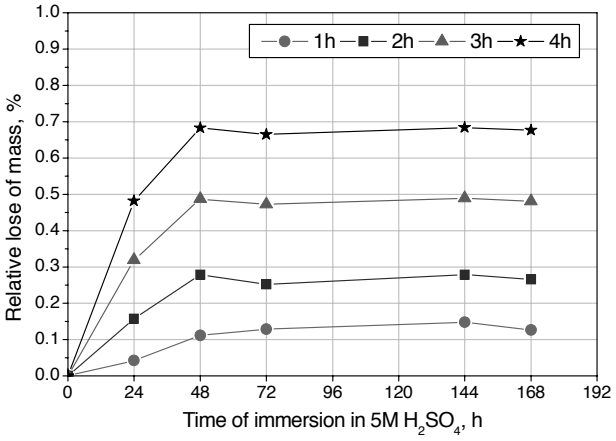

Fig. 20. The relative lose of mass during immersion test in 5M H_2SO_4 of samples sintered for different time periods

The immersion test in sulfuric acid solution (Fig. 20) revealed higher corrosion resistance of samples sintered for 1h thus with higher austenite content in the microstructure despite of the lower density of such samples. After first 24 hours the samples surface became covered by black deposited, especially sample sintered for 1h. The black coloured film can be associated with the formation of nickel sulphide on the metal surface [14,15]. This film can be very stable and passive and thus could increase the corrosion resistance. The corrosion in sulphuric acid proceed through uniform corrosion, where preferentially ferritic phase become dissolved and austenitic one enriched in nickel resist corrosion attack.

4. Conclusions

The sintering time greatly influences the properties of PM duplex stainless steel. Studies of the influence of sintering time (in range of 1 to 4h) on the properties of PM duplex stainless steels can be summarised as follows:

a) Increase of sintering time from 1 to 4 h result in density growth from 7.14 g/cm^3 to 7.40 g/cm^3. The effect of sintering cycle on pore morphology is more evident in the pore shape factor f_s than f_c, that both are shifted towards higher values that confirm lower pore elongation and their higher regularity with prolonged sintering time.

b) The austenite in microstructure is located along prior ferritic grain boundaries and occurs as intra-granular austenite side plates. Prolonged sintering time results progressive development of cellular austenite grains. The balance between both phases in duplex microstructure was obtained when sintering time of 3h and more was applied. Prolonged sintering time result in segregation of austenite and ferrite former elements in respective phases. The partition coefficients k_{Mo} tend to increase while nickel partition coefficient (k_{Ni}) decrease with sintering time.

c) The mechanical properties of sintered duplex stainless steels grow with prolonged sintering time. Tensile properties progressively increased from R_m=680MPa to 760MPa after 4h of sintering, while the elongation increased from 14 to 18%.

The highest effect of sintering time was visible for impact strength values that raised more than 200% from 95J to 227J. Elongation of sintering time cause increase in portion of plastic zones and connections between powder particles and improve pore morphology that have great impact on the toughness of sintered materials. Fracture of studied steels has a mixed type of ductile and brittle fracture and presents the dimples type rapture.

d) PM duplex stainless steels sintered for longer times exhibited lower corroded surface area in NaCl salt spray test, where the porosity plays dominant role in corrosion initiation. In the environment of sulfuric acid microstructures with higher austenite content showed better performance than balanced duplex microstructure.

Acknowledgements

Presented researches were partially funded by the Polish Ministry of Science and Higher Education as a research project No. N N507 470137.

The authors are indebted to the technical staff of Mechanical Laboratory of Alessandria Campus of the Politecnico di Torino for their contribution to materials testing.

References

[1] C.J. Munez, M.V. Utrilla, A. Urena, Effect of temperature on sintered austeno-ferritic stainless steel microstructure, Journal of Alloys and Compounds 463 (2008) 552-558.

[2] R. Mariappan, S. Kumaran, T. Srinivasa Rao, Effect of sintering atmosphere on structure and properties of austeno-ferritic stainless steel, Materials Science and Engineering A 517 (2009) 328-333.

[3] Hwan-Jin Sung, Tae Kwon Ha, Sangho Ahn, Young Won Chang, Powder injection molding of a 17-4 PH stainless steel and the effect of sintering temperature on its microstructure and mechanical properties, Journal of Materials Processing Technology 130-131 (2002) 321-327.

[4] L.A. Dobrzański, Z. Brytan, M.A. Grande, M. Rosso, E.J. Pallavicini, Properties of vacuum sintered duplex stainless steel, Journal of Materials Processing Technology 162-163 (2005) 286-292.

[5] L.A. Dobrzański, Z. Brytan, M. Actis Grande, M. Rosso, Corrosion resistance of sintered duplex stainless steels in the salt fog spray test, Journal of Materials Processing Technology 192-193 (2007) 443-448.

[6] L.A. Dobrzański, Z. Brytan, M. Rosso, Sinter-hardening process applicable to stainless steels, Journal of Achievements in Materials and Manufacturing Engineering 24/2 (2007) 11-18.

[7] C. Garcia, F. Martin, P. de Tiedra, L. Garcia Cambronero, Pitting corrosion behaviour of PM austenitic stainless steels sintered in nitrogen–hydrogen atmosphere, Corrosion Science 49 (2007) 1718-1736.

[8] C. Moral, A. Bautista, F. Velasco, Aqueous corrosion behaviour of sintered stainless steels manufactured from mixes of gas atomized and water atomized powders, Corrosion Science 51 (2009) 1651-1657.

[9] C. Garcia, F. Martin, Y. Blanco, M.P. de Tiedra, M.L. Aparicio, Corrosion behaviour of duplex stainless steels sintered in nitro gen, Corrosion Science 51 (2009) 76-86.

[10] T. Marcu Puscas, M. Signorini, A. Molinari, G. Straffelini, Image analysis investigation of the effect of the process variables on the porosity of sintered chromium steel, Materials Characterization 50 (2003) 1-10.

[11] H.C. Pavanati, A.M. Maliska, A.N. Klein, J.L.R. Muzart, Comparative study of porosity and pore morphology of unalloyed iron sintered in furnance and plasma reactor, Materials Research 10/1 (2007) 87-93.

[12] B. Kubicki, Stress Concentration at Pores in Sintered Materials, Powder Metallurgy 38/4 (1995) 295- 298.

[13] B.D. Cullity, Elements of x-ray diffraction, Second Edition, Addison-Wesley Publishing Company, Inc., 1978.

[14] Y. Li, M.B. Ives, K.S. Coley, J.R. Rodda, Corrosion of nickel – containing stainless steel in concentrated sulphuric acid, Corrosion Science 46 (2004) 1969-1979.

[15] J.H. Potgieter, P.A. Olubambi, L. Cornish, C.N. Machio, El-Sayed M. Sherif, Influence of nickel additions on the corrosion behaviour of low nitrogen 22% Cr series duplex stainless steels, Corrosion Science 50 (2008) 2572-2579.